TWMS J. App. Eng. Math. V.1, N.2, 2011, pp. 127-149

MATHEMATICAL MODELING OF THE DISSOLUTION PROCESS OF SILICON INTO GERMANIUM MELT

F. MECHIGHEL[1], N. ARMOUR[2], S. DOST[2], M. KADJA[3] §

Abstract. Numerical simulations were carried out to study the thermosolutal and flow structures observed in the dissolution experiments of silicon into a germanium melt. The dissolution experiments utilized a material configuration similar to that used in the Liquid Phase Diffusion (LPD) and Melt-Replenishment Czochralski (Cz) crystal growth systems. In the present model, the computational domain was assumed axisymmetric. Governing equations of the liquid phase (Si-Ge mixture), namely the equations of conservation of mass, momentum balance, energy balance, and solute (species) transport balance were solved using the *Stabilized* Finite Element Methods (ST-GLS for fluid flow, SUPG for heat and solute transport).
Measured concentration profiles and dissolution height from the samples processed with and without the application of magnetic field show that the amount of silicon transported into the melt is slightly higher in the samples processed under magnetic field, and there is a difference in dissolution interface shape indicating a change in the flow structure during the dissolution process. The present mathematical model predicts this difference in the flow structure. In the absence of magnetic field, a flat stable interface is observed. In the presence of an applied field, however, the dissolution interface remains flat in the center but curves back into the source material near the edge of the wall. This indicates a far higher dissolution rate at the edge of the silicon source.

Keywords: Dissolution, convection, diffusion, numerical simulation, stabilized finite element techniques.

AMS Subject Classification: 76M10

1. Introduction

The melt/solution of a crystal growth process exhibits complex transport phenomena involving momentum, energy, and solute (mass) under applied thermal profiles and the presence of an applied magnetic fields further complicates the phenomena [1]. All these phenomena have in common that they are modeled by transport equations with nonlinear source terms [2]. Indeed, under certain assumptions, mathematically, these phenomena could be governed by partial differential equations (PDEs). For instance, the Navier-Stokes equation for viscous incompressible fluid flow, the advection-conduction equation for energy conservation, and the advection-diffusion equation for solute transport are good

[1] University of Limoges, SPCTS UMR CNRS 6638, Eur. Centre for Ceramics, Limoges, France, University of Constantine, Mechanical Engineering Department, Constantine, Algeria, e-mail: farid.mechighel@etu.unilim.fr
[2] Crystal Growth Laboratory, University of Victoria, Victoria, BC, Canada, e-mail: sdost@me.uvic.ca; Corresponding Author
[3] University of Constantine, Mechanical Engineering Department, Constantine, Algeria
§ Manuscript received 16 October 2011.

model equations for these phenomena [1, 2]. Moreover, in order to ensure the growth of a single crystal with high quality, these phenomena must be controlled and thus experiments must be complimented by numerical simulations in order to achieve optimal growth conditions [1, 3, 4, 5, 6, 7, 8].

As computers and computational fluid dynamics (CFD) tools (numerical methods) have become more popular and widespread; there is a growing demand for solving such complex transport phenomena problems. The finite element method (FEM) is considered as one of the most promising tools to handle these problems numerically [2, 9].

Although application of the *classical Galerkin FEM* for solving common problems, such as those in structural mechanics and heat conduction, has had notable success, CFD still encounters some open and not well-handled problems. One of them is the reliable modeling of convection-dominated transport phenomena (for instance, incompressible flows at high Reynolds numbers, convection-dominated diffusion heat transport, etc.), which often appear in a variety of applications including crystal growth and solidification [10, 11]. The main difficulty is due to the presence of convection operators (non-linear) in the formulation of flow problems based on kinematical descriptions other than Lagrangian [10, 12]. In fact, convection operators are non-symmetric and thus the best approximation property in the energy norm of the Galerkin finite element method is lost when convection dominates the transport process[10].

Generally, solutions to convection-dominated transport problems by the standard Galerkin method are often polluted by spurious node-to-node oscillations. These may only be removed by mesh and time-step refinement which obviously makes the use of the method impractical [10]. This has motivated the development of alternatives to the standard Galerkin formulation which prevent such oscillations without requiring mesh or time-step refinement. Such alternatives are called *stabilization* methods and have demonstrated a major issue breakthrough in finite element modeling of convection-dominated transport problems [10, 11].

Several stabilized finite element techniques are seen in the literature. The mainly utilized stabilized methods are the Streamline-upwind/Galerkin (SUPG) method [10, 13, 14], the Space-time Galerkin/least-squares (ST-GLS) method [10, 15, 16, 17], the Subgrid scale (SGS) method [2, 17, 18], the Taylor-Galerkin (TG) method [10, 19, 20], among others. Some of these methods have the transient problem as starting point, whereas the others are developed by considering first the *stationary* equations [20]. Stabilized finite elements are constructed based on the simple idea that one can modify the variational (weak) form of a particular problem in order to improve numerical stability without compromising consistency or accuracy. Indeed, all these methods consist of adding in a stabilizing term to the original Galerkin formulation (weak form) of the problem [10, 20]. This stabilizing term is multiplied by a numerical parameter called stabilization parameter [20]. Different methods differ in the manner the operator acts on the test function and in the design of the algorithmic parameter. The literature of the stabilized FEM techniques is very rich, and almost all studies on this subject have considered handling incompressible fluid flows or advection-diffusion-reaction problems. Only a small number of those have tackled problems in industrial applications like solidification and crystal growth (in which such problems are coupled).

The present study was performed with the objective of using the ST-GLS and SUPG finite element techniques. These are developed to compute the fluid flow and/or advection-diffusion-reaction problems and handle the coupling problem of transport phenomena in the dissolution process. Recently, dissolution experiments were performed in a crucible similar to that used in an LPD or Melt-Replenishment Czochralski (Cz) growth system

[8] (schematically shown in Figure 1). In the present modeling study, we have considered an axisymmetric domain in modeling the material configuration of this dissolution process as seen in Figure 1. The silicon source is placed at the top of the melt, and the silicon source dissolves into germanium melt under an applied temperature profile in the opposite direction to the gravity-induced buoyancy force. Due to the large density difference between the silicon solute and the germanium-rich melt, the lighter silicon solute is buoyant, and the diffusion of silicon acts to stabilize the melt against natural convection. This configuration is very stable and used for crystal growth of SiGe.

2. Model Description and the Governing Equations

The setup used in the simulation is the arrangement in which the silicon seed is floating on top of the germanium melt. In this case, the silicon seed covers the melts free surface. This arrangement is similar to that used in the liquid phase diffusion (LPD) growth system for SiGe [21]. A schematic of the material configuration used in this work is shown in Figure 2. This configuration was numerically simulated. The field equations of the liquid phase (Navier-Stokes, energy and species transport equations) are written in cylindrical coordinates and solved by the finite element technique under the assumption of axisymmetry.

In the simulation the following initial and boundary conditions are adopted:

- *Thermal conditions:* Initially, the domain is at 800^oC. It is then suddenly immersed into an 1100^oC isothermal region. The temperature boundary conditions are applied to all domain boundaries except the top (source and quartz wall), where the heat flux is set to be zero.
- *Flow conditions:* The domain is initialized at zero velocity. The crucible wall and the dissolution interface are considered as a no-slip boundary condition.
- *Concentration conditions:* The germanium melt domain is initialized at zero silicon concentration, and the boundary between germanium melt and silicon is at the saturation concentration.

In addition, we made the following assumptions regarding the solid silicon source and the germanium melt. The thermo-physical properties, such as the thermal conductivity k_L, the dynamic viscosity μ_L, the thermal diffusivity $\alpha_L = k_L/\rho_L cp$, and the diffusion coefficient D_L of the melt, are constants. The flow is laminar. The melt is a Newtonian, viscous, incompressible fluid mixture. There is no viscous dissipation and the Boussinesq approximation holds. For the silicon solid, thermo-physical properties, such as the thermal conductivity k_S, and the thermal diffusivity $\alpha_S = k_S/\rho_S cp_S$, are taken as constants. In the solid no species diffusion ($D_S \approx 0$) is considered. The material's (silicon, germanium, vacuum and quartz) thermo-physical data are taken from the following references [22, 23, 24].

Figure 2 shows schematically the vertical cross section of the present dissolution system. Under the above assumptions, the three-dimensional time-dependent governing equations describing the fluid flow, heat and solute transport for the liquid phase are written in cylindrical coordinates $\mathbf{x}(r, \varphi, z)$. It is easy to write two-dimensional (axisymmetric) equations from the three dimensional equations by simply dropping the dependency on the azimuthal angle (φ) in the field dependent variables. The growth cell is assumed axisymmetric with respect to the centerline (z-axis) as shown in Figure 2. However, it is necessary to introduce additional boundary conditions for the imposed axisymmetry condition.

2.1. **Further Considerations on the Model Setup.**

As shown in Figure 2, we assume that the setup may be subdivided into:

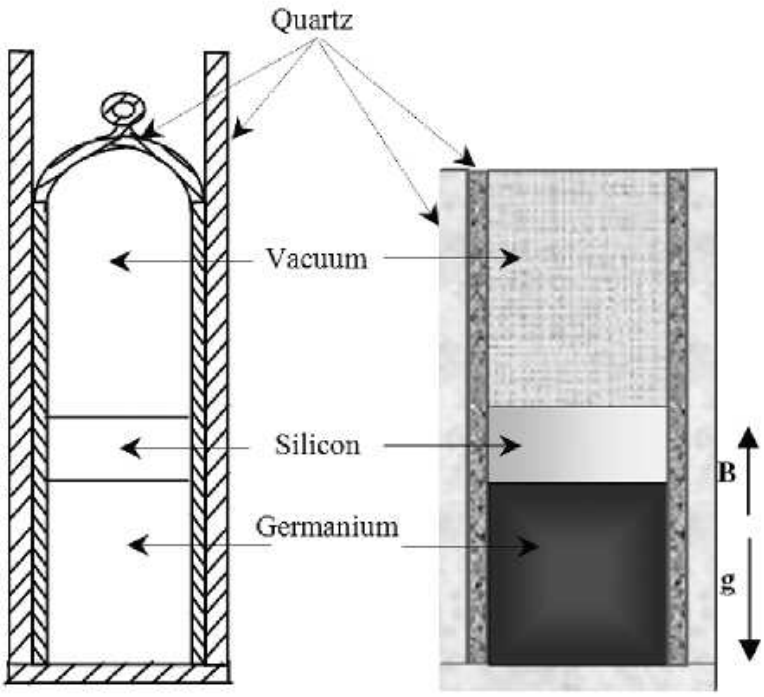

FIGURE 1. Schematic of the physical domain (left). Experimental setup, (right) Simulated domain.

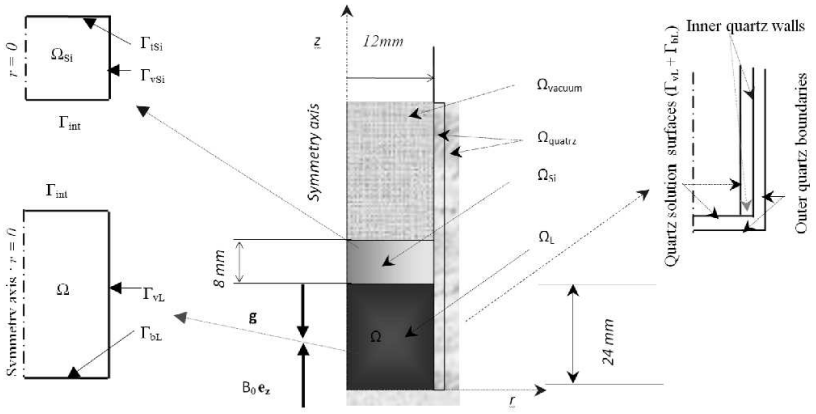

FIGURE 2. The axisymmetric model domain geometry with finite element notation.

- A liquid phase. This phase is composed of the following subdomains. The domain $(\Omega_t)_1$ for the solution (Si/Ge), and the domain $(\Omega_t)_2$ for the silicon solid (modeled here as fluid with infinite viscosity $\mu_{Si} \gg 1$, (hence $\mathbf{u} = \mathbf{u}_s \approx 0$ velocity vector in the silicon), moreover no mass diffusion in the silicon phase $D_{Si} \ll 1$). The Navier-Stokes equations, concentration conservation equation and energy conservation (of course) may be applied in this domain. The interface between $(\Omega_t)_1$ and $(\Omega_t)_2$ is denoted by Γ_{int}. Thus we have: $(\Omega_t)_{total}$=$(\Omega_t)_1$ +$(\Omega_t)_2$.

- Solid phases. These consist of the quartz material in the subdomain space denoted by Ω_{quartz}. As we are only concerned with the transport phenomena in the SiGe melt, only the subdomain $(\Omega_t)_L$ will be considered and, for simplicity, it will be denoted by Ω_t. The boundary of this domain will be denoted by Γ_t.

For simplicity, we drop the subscript t. Therefore, from Figure 2, the SiGe melt (liquid) Ω_L has a boundary Γ_L. Γ_L consists of the dissolution interface Γ_{int}, the crucible vertical wall Γ_{vL} and the crucible bottom wall Γ_{bL}. This domain has a symmetry boundary at $r = 0$. The silicon solid domain Ω_{Si} has a boundary Γ_{Si}. This boundary consists of the dissolution interface Γ_{int}, the vertical crucible wall Γ_{vSi} and the top boundary Γ_{tSi}. The silicon solid domain has a symmetry axis at $r = 0$. The other solid materials are denoted by the domain Ω_S (representing the quartz and vacuum) with a boundary denoted Γ_S. The quartz domain has a boundary Γ_{quartz} which consists of outer crucible boundaries (ampoule), inner quartz boundaries (ampoule-crucible), and inner quartz walls (crucible-solution). For simplicity, we assume perfect thermal contact at all internal boundaries. Therefore, at these boundaries, the heat flux is continuous.

2.2. **Governing Equations of the Liquid Phase.**

2.2.1. *Momentum Transport (unsteady Navier-Stokes equations).* Mathematically, Figure 2 may be viewed as a flow region Ω_t in $R^{n_{sd}}$ which represents the spatial domain (Ω) at time $t \in [0, t_{max}]$, where n_{sd} is the number of space dimensions $n_{sd} = 2$ (axisymmetric case) or $n_{sd} = 3$. The domain Ω_t occupied by the fluid at t is assumed bounded (finite size). Γ_t is the boundary of the fluid domain Ω_t which is assumed to be *Lipschitz* continuous, meaning that it is a closed and sufficiently regular surface. The section of the boundary at which the velocity components (similar for temperature, or species concentration) are prescribed (essential condition) is denoted by $(\Gamma_t)_D$. The Neumann (natural) boundary conditions are imposed at the remaining part of the boundary $(\Gamma_t)_N$.

Then, under the above assumptions, the principles of conservation of mass and balance of momentum yield the following continuity and momentum equations (time-dependent Navier-Stokes equations) [23], in which the velocity-pressure formulation is adopted:

$$\nabla \cdot \mathbf{u} = 0 \,\text{on}\, \Omega_t,\ \forall t \in (0, t_{max}) \tag{1}$$

$$\rho \frac{\partial \mathbf{u}}{\partial t} + \rho(\mathbf{u} \cdot \nabla)\mathbf{u} - \nabla \cdot \boldsymbol{\sigma} = \mathbf{F} \,\text{on}\, \Omega_t,\ \forall t \in (0, t_{max}) \tag{2}$$

where, ρ , $\mathbf{u}(\mathbf{x}, t)$, with $\mathbf{x}(r, \varphi = 0, z)$ are the fluid density (satisfying the Boussinesq approximation), mass average velocity vector (which has a radial and an axial component denoted by u and v) and the position vector (note that for an axisymmetric flow field expressed in terms of the cylindrical coordinate system $\mathbf{x}(r, \varphi, z)$, all flow variables are independent of the azimuthal angle φ). Also, $\mathbf{F}(\mathbf{x}, t) = \rho\mathbf{g} + \mathbf{F}_L$ represents the external body forces, which includes the contributions of both the gravitational body force or buoyancy force, $\mathbf{F}_{buoy} = \rho\mathbf{g}$), and the magnetic body force, $\mathbf{F}_L$. Note that the bold face letters are used to denote vectors, matrices or tensors.

Using Stokes' law which states that, for an incompressible and Newtonian fluid, the stress tensor is given by $\boldsymbol{\sigma}(p, \mathbf{u}) = -p\mathbf{I} + 2\mu\boldsymbol{\epsilon}(\mathbf{u})$, where the rate of deformation tensor $\boldsymbol{\epsilon}(\mathbf{u}) = \frac{1}{2}[\nabla\mathbf{u} + (\nabla\mathbf{u})^T]$, (the symmetric part of the velocity gradient), with p the pressure, and $\mathbf{I}$ the identity tensor.

For the flow velocity field, the homogeneous Dirichlet condition (no-slip) was assumed on the solution-crucible boundaries (i.e. the crucible vertical and bottom surfaces on the

liquid side $\Gamma_{bL} + \Gamma_{vL}$). This is also the condition on the dissolution interface and will be shown later.

$$\mathbf{u}(\mathbf{x}, t) = \mathbf{u}_D(\mathbf{x}, t) = \mathbf{0} \,\text{on}\, (\Gamma_t)_D, \, \forall t \in (0, t_{max}) \tag{3}$$

where $\mathbf{u}_D(\mathbf{x}, t) = \mathbf{0}$ is a specified condition (Dirichlet boundary condition) on the liquid region boundaries. Here, $(\Gamma_t)_D = \Gamma_t$ and $(\Gamma_t)_N = \boldsymbol{\phi}$.

For the initial condition at $t = 0$, the velocity field was specified as $\mathbf{u}_0(\mathbf{x}) = 0$. This is the divergence free velocity field, i.e. $\nabla \cdot \mathbf{u}_0 = 0$, over the domain Ω_t.

$$\mathbf{u}(\mathbf{x}, 0) = \mathbf{u}_0(\mathbf{x}) = \mathbf{0} \,\text{on}\, \Omega_0 \tag{4}$$

Finally the system of Navier-Stokes equations, Equations 1 and 2, governing the unsteady incompressible fluid flow in the melt and the associated with suitable initial and boundary conditions, Equations 3 and 4, form a well-posed initial boundary value problem, which can be handled using the finite element method.

We then assume that the spatial domain is fixed in time under this assumption and the subscript t is dropped from the symbols Ω_t, and Γ_t.

2.2.2. *EnergyTransport (Unsteady Advection-Conduction Equation).* The balance of thermal energy over the domain Ω with the boundary Γ leads to the following time-dependent advection-diffusion equation [23],

$$\frac{\partial T}{\partial t} + \mathbf{u} \cdot \nabla T - \nabla \cdot (\alpha_L \nabla T) = 0 \,\text{on}\, \Omega \,\text{and}\, \forall t \in (0, t_{max}) \tag{5}$$

Neither heat generation (Joule heating) nor absorption are considered. It is also assumed there is no heat transfer by radiation. T represents the temperature, α_L is the thermal diffusivity of the fluid (constant).

The temperature boundary condition on the melt-crucible boundaries (Γ_{bL} and Γ_{vL}) is continuity, which can be written as $\mathbf{n} \cdot (\mathbf{q}_1 - \mathbf{q}_2) = 0$. $\mathbf{n}$ is the exterior unit normal to the boundary and $\mathbf{q}_i = -k_i \nabla T_i$ (where, i refers to material 1 and material 2, i.e. silicon/solution and quartz/solution).

On liquid/crucible boundaries which represent the interior boundaries for the temperature field, the continuity condition is used. In absence of heat sources and sinks (as assumed for this model), the continuity condition reads,

$$\mathbf{n} \cdot (\mathbf{q}_1 - \mathbf{q}_2) = 0 \quad \text{on all internal boundaries, } \forall t \in (0, t_{max}) \tag{6}$$

This means that the heat flux in the normal direction is continuous across the boundary. This is valid given the previous assumption of perfect thermal contact. Equation 6 may be written as, $\mathbf{n} \cdot (\mathbf{q}_1 - \mathbf{q}_2) = (h_T)_1 - (h_T)_2 = h_T = 0$ on Γ_N ($\Gamma_N = \Gamma - \Gamma_{int}$). The temperature boundary conditions an the dissolution and symmetry boundaries will be illustrate later. The condition $T_{ini} = 800^o C$ was specified as the initial condition. This may be written as,

$$T(\mathbf{x}, 0) = T_0(\mathbf{x}) = T_{ini} \,\text{on}\, \Omega_0 \tag{7}$$

The time-dependent advection-conduction equation, Equation 5, governing the heat transport in the crucible associated with the suitable initial and boundary condition equations, Equations 6 and 7, represent a well-posed initial boundary value problem.

2.2.3. *Solute Transport (Unsteady Advection-Diffusion Equation).* Assuming that the crucible wall is not permeable, and there is no solute (silicon) diffusion in the solid ($D_S \ll D_L$), the solute transport may be given by the following time-dependent advection-diffusion equation [23].

$$\frac{\partial C}{\partial t} + \mathbf{u} \cdot \nabla C - \nabla \cdot (D_L \nabla C) = 0 \,\text{on}\, \Omega \,\text{and}\, \forall t \in (0, t_{max}) \tag{8}$$

where C and D_L represent silicon (solute) concentration and the diffusion coefficient of silicon in the Si-Ge liquid mixture. It is assumed that all melt-crucible boundaries (Γ_{bL} and Γ_{vL}) are not permeable for species transport, therefore the solutal boundary conditions associated with Equation 8 are given by,

$$\mathbf{n} \cdot D_L \nabla C = h_C = 0 \,\text{on}\, \Gamma_N,\ \forall t \in (0, t_{max}) \tag{9}$$

where, $h_C = 0$ means that the species flux is set to zero (Neumann condition) on all the liquid region boundaries excluding the dissolution interface. Here, $\Gamma_N = \Gamma - \Gamma_{int}$. On Γ_{int}, a Dirichlet condition is imposed and is illustrated later. Equation 9 may be written in terms of diffusive and convective fluxes $\mathbf{n} \cdot (-D_L \nabla C + C\mathbf{u}) = 0$. As the no-slip condition for the velocity was imposed on the crucible boundaries, this equation reduces to the form stated in Equation 9.

$$C(\mathbf{x}, 0) = C_0(\mathbf{x}) = 0 \,\text{on}\, \Omega_0 \tag{10}$$

The unsteady advection-diffusion equation, Equation 8, governing the solute transport in the crucible together with suitable initial and boundary condition equations, Equations 9 and 10, represent a well-posed initial boundary value problem.

Remark 1: Note that in the cylindrical coordinate system (under the hypothesis of axisymmetry) for the velocity vector denoted by $\mathbf{u} = (u, w, v)^T$, with f representing quantities such as (u, v, w, p, T or C), we have,

$$\nabla \cdot \mathbf{u} = \frac{1}{r}\frac{\partial}{\partial r}(ru) + \frac{1}{r}\frac{\partial w}{\partial \varphi} + \frac{\partial v}{\partial z} = \frac{1}{r}\frac{\partial}{\partial r}(ru) + \frac{\partial v}{\partial z} \tag{11}$$

$$\nabla f = \frac{\partial f}{\partial r}\mathbf{e}_r + \frac{1}{r}\frac{\partial f}{\partial \varphi}\mathbf{e}_\varphi + \frac{\partial f}{\partial z}\mathbf{e}_z = \frac{\partial f}{\partial r}\mathbf{e}_r + \frac{\partial f}{\partial z}\mathbf{e}_z \tag{12}$$

$$\nabla^2 f = \nabla \cdot \nabla f = \frac{1}{r}\frac{\partial}{\partial r}\left(r\frac{\partial f}{\partial r}\right) + \frac{1}{r^2}\frac{\partial}{\partial \varphi}\left(\frac{\partial f}{\partial \varphi}\right) + \frac{\partial}{\partial z}\left(\frac{\partial f}{\partial z}\right) = \frac{1}{r}\frac{\partial}{\partial r}\left(r\frac{\partial f}{\partial r}\right) + \frac{\partial^2 f}{\partial z^2} \tag{13}$$

2.2.4. *Electric Charge Balance Equation and the Magnetic Body Force.* The crucible is subjected to an applied axial static (steady) magnetic field $\mathbf{B} = B_0\mathbf{e}_z$ with a uniform field intensity of B_0 as shown in Figure 2. For metallic liquids, the magnetic body force $\mathbf{F}_L$ acting on the points of the liquid $\mathbf{x} \in \Omega$ (spatial domain) may be taken simply as,

$$\mathbf{F}_L = \mathbf{J} \times \mathbf{B} \tag{14}$$

where the contribution of electric charge is neglected, and the current density is given by Ohms law.

$$\mathbf{J} = \sigma_e(-\nabla\phi + \mathbf{u} \times \mathbf{B}) \tag{15}$$

The current density $\mathbf{J}$ is governed by the conservation of current,

$$\nabla \cdot \mathbf{J} = 0 \tag{16}$$

Equation 16 assumes that the induced fields due to the applied magnetic field are negligible. This is a good approximation for metallic liquids since the magnetic Reynolds numbers are sufficiently small [25, 26]. In the above equations ϕ is the electric potential and σ_e the electric conductivity of the liquid phase. In this case, the magnetic body force becomes,

$$\mathbf{F}_L = \sigma_e(-\nabla\phi + \mathbf{u} \times \mathbf{B}) \times \mathbf{B} \tag{17}$$

Combining Equation 14 and Equation 15 leads to the following Poisson equation,

$$\nabla^2\phi = \nabla \cdot (\mathbf{u} \times \mathbf{B}) = B_0\mathbf{e}_z \cdot (\nabla \times \mathbf{u}) = S_\phi \,\text{on}\, \Omega \tag{18}$$

This governs the electric potential distribution.

Since it is assumed an electrically insulated boundary, the normal derivative of ϕ is prescribed on the Neumann portion, Γ_N, of the boundary Γ and thus $\Gamma_N = \Gamma$.

$$\mathbf{n} \cdot \nabla\phi = h_\phi = 0 \,\text{on}\, \Gamma_N \tag{19}$$

The Poisson equation, Equation 18, and the associated with the boundary condition equation, Equation 19, form a well-posed boundary value problem, which may be solved easily with the classical Galerkin finite element method. Note that since the vorticity vector $\nabla \times \mathbf{u} = (\partial u/\partial z - \partial v/\partial r)\mathbf{e}_\varphi$ under the axisymmetry assumption, the electrical potential conservation equation reduces to $\nabla^2\phi = 0$. This simplifies significantly the problem and the resolution of this equation is not required as there is no contribution of gradient of ϕ in the magnetic body force (i.e. $\mathbf{F}_L = \sigma_e(\mathbf{u} \times \mathbf{B}) \times \mathbf{B}$).

2.2.5. *Interface Condition.* We assume that the dissolution interface (solid silicon-liquid SiGe mixture) is flat, stationary and that local thermodynamic equilibrium is reached. The concentration at the dissolution interface is determined from the SiGe binary phase diagram namely, a function $C_{eq}^L = C_{sat} = fn(T_{eq})$. On the dissolution interface we adopt the following saturation concentration (in molar concentration of silicon) predicted from the SiGe phase diagram.

$$C_{eq}^L = C_{sat} = 2005.6256 \times \left[\frac{(cc \times 28.086)}{(72.64 \times (1.0 - cc) + 28.086 \times cc)}\right] \tag{20}$$

where,

$$cc = [4 \times 10^{-6} \times (T - 273.15)^2 - 0.007 \times (T - 273.15) + 3.361] \tag{21}$$

2.2.6. *Boundary Conditions on the Dissolution Interface.* At the dissolution interface Γ_{int}, namely, we assume that the concentration is in equilibrium, and since the experimentally observed dissolution rate of silicon source into the solution is very small (approximately 0.3 mm/day), the velocity components (u, v) of fluid particles at the dissolution interface are vanished (thus $\mathbf{u} = \mathbf{u}_{int} \cong \mathbf{0}$) [8, 23]. Furthermore, we assume that between the liquid and the dissolution interface the heat flux is continuous (continuity condition), and the concentration balance equation at the dissolution interface can be excluded from the consideration [8, 23]. Thus, for equilibrium concentration, flow and energy balance we can write,

$$C = C_{dis}^L = C_{eq}^L,\ (u = 0 \text{ and } v = 0) \text{ and } k_{Si}\frac{\partial T_S}{\partial \mathbf{n}} - k_L\frac{\partial T_L}{\partial \mathbf{n}} = 0 \tag{22}$$

where C_{dis}^L is the equilibrium concentration of the solute (silicon) at the dissolution interface (silicon/solution). k_L and k_{Si} are the thermal conductivities of the SiGe solution and silicon solid. T_S and T_L are the temperatures referred to the silicon solid and the liquid solution respectively. $\partial/\partial\mathbf{n}$ stands for the derivative of the exterior unit normal to the boundary.

At the dissolution interface, we assume local thermodynamic equilibrium is reached. This implies that the temperature at Γ_{int} is set by the SiGe solution equilibrium phase diagram as $T = T_{melt} = T_{eq}$, which stands in fact a Dirichlet type boundary condition (denoted by $g_T(\mathbf{x}, t)$ or $T_D(\mathbf{x}, t)$) on the interface.

These conditions along with the symmetry boundary conditions, which are shown later, represent the closure relations for the solution of the liquid phase of our problem. These may be written for the finite element implementation as,

$$C(\mathbf{x}, t) = g_C(\mathbf{x}, t) = C_{sat} \text{ on the dissolution interface } \Gamma_D = \Gamma_{int},\ \forall t \in (0, t_{max}) \tag{23}$$

$$\mathbf{u}(\mathbf{x}, t) = \mathbf{u}_D(\mathbf{x}, t) = \mathbf{0} \text{ on the dissolution interface } \Gamma_D = \Gamma_{int},\ \forall t \in (0, t_{max}) \tag{24}$$

$$T(\mathbf{x}, t) = g_T(\mathbf{x}, t) = T_{eq} \text{ on the dissolution interface } \Gamma_D = \Gamma_{int},\ \forall t \in (0, t_{max}) \tag{25}$$

2.2.7. *Boundary Conditions at the Axis of Symmetry.* At the axis of symmetry, we use symmetry boundary conditions. For physical (finite) results, it is required that the radial velocity component be zero [23]. Therefore, we have,

$$u = 0 \text{ and } \frac{\partial v}{\partial r} = 0 \text{ on the symmetry axis } (r = 0),\ \forall t \in (0, t_{max}) \tag{26}$$

$$\mathbf{n} \cdot \alpha_L \nabla T = h_T = 0 \text{ on the symmetry axis } (r = 0),\ \forall t \in (0, t_{max}) \tag{27}$$

$$\mathbf{n} \cdot D_L \nabla C = h_C = 0 \text{ on the symmetry axis } (r = 0),\ \forall t \in (0, t_{max}) \tag{28}$$

2.3. **Solid phases.** Based on experimental results, we assume that there is no species diffusion in the solids such that $\mathbf{u}_S = 0$ (where $\mathbf{u}_S$ velocity vector in the solid phases) [23]. Therefore, the only additional equation needed is the energy balance given by,

$$\frac{\partial T}{\partial t} = \frac{k_S}{\rho_S cp_S}\nabla^2 T \text{ on } \Omega_S,\ \forall t \in (0, t_{max}) \tag{29}$$

where ρ_S, cp_S, and k_S are the density, specific heat and thermal conductivity of the solid material, respectively. Note that solid phases in the model are the solid silicon, the quartz or the vacuum as diagrammed in Figure 1.

In the silicon solid phase, Ω_S represents Ω_{quartz}. The equilibrium condition on Γ_{int}, the continuity conditions on crystal-crucible boundary (the crucible wall on the silicon solid side Γ_{vS}) and the top crystal-vacuum boundary Γ_{vS} together provide the required boundary conditions for solution of the heat transport problem.

For the quartz crucible, Ω_S represents Ω_{quartz}. The thermal boundary conditions for the outer vertical wall, and bottom surface of the quartz crucible are expressed as a specified temperature $T = 1100^oC$. At the top surface of the domain the flux was set to zero.

Perfect thermal contacts and continuous heat flux at the silicon-crucible, solution-crucible and inner crucible boundaries was assumed as before.

3. Mathematical Background - Numerical Resolution and Finite Element Formulations

The application of the finite element method for solving an initial boundary value problem requires a certain concepts that are illustrated in the following section. The initial boundary value problems are described by Equations 1 to 4, Equations 5 to 7 and Equations 8 to 10. These equations along with their associated boundary and initial conditions are discussed in the context of a finite element method solution.

3.1. Basic Issues of the Finite Element Method.

The procedure of spatial discretization by the finite element method rests upon the discrete representation of a so-called *weak integral form* of the partial differential equation (PDE). The *formulation* and consequent *discretization* of such an *integral form* requires the definition of some *function spaces* and associated *norms*.

For simplicity, we consider here the *steady state* version of the equations (for energy or solute transport). Consider the domain $\Omega \subset R^{n_{sd}}$ with the *piecewise* smooth *boundary* Γ. Here again, $n_{sd} = 2$ denotes the number of space dimensions. We use the notation of $f : \hat{\Omega} \rightarrow R$, (where here $f = T$ or C) to state that for each *spatial point* $\mathbf{x}(r, z) \in \hat{\Omega}$, $f(\mathbf{x}) \rightarrow R$, where $\hat{\Omega}$ denotes the *closure* of Ω, (with $\hat{\Omega} = \Omega \cup \Gamma$).

Definition 1: A *scalar function* $f : \hat{\Omega} \rightarrow R$ is said to be of class $C^m(\Omega)$ if all its *derivatives* up to order m exist and are *continuous* functions. In finite element analysis, we use *integral equations* and we are interested in *functions* belonging to larger spaces than C^m. Instead of requiring the *m-th* derivative to be *continuous*, we require that its *square* is *integrable*. In fact, *finite element functions* should possess generalized derivatives and some integrability properties. Such classes of functions are *particular* examples of the *Sobolev* function spaces [10].

Definition 2: ***(Sobolev Spaces for Scalar Functions):*** For any non-negative *integer* k, one can define the *Sobolev* space $H^k(\Omega)$ using multi-index notation. Given the *n-tuple* $\alpha = (\alpha_1, \alpha_2, ..., \alpha_{n_{sd}}) \in N^{n_{sd}}$, and the non-negative *integer* $|\alpha| = \alpha_1 + \alpha_2 + ... + \alpha_{n_{sd}}$, we define the *Sobolev space functions (scalar)* as,

$$H^k(\Omega) = \left\{ f \in L^2(\Omega) | \frac{\partial^{|\alpha|} f}{\partial x_1^{\alpha_1} \partial x_2^{\alpha_2} ... \partial x_{n_{sd}}^{\alpha_{n_{sd}}}} \in L^2(\Omega) \ \forall |\alpha| \leq k \right\} \tag{30}$$

where $L^2(\Omega)$ denotes the space of functions that are *square integrable* over the domain Ω. Therefore, $H^k(\Omega)$ consists of square integrable functions all of whose derivatives of order up to k are also square integrable. $H^k(\Omega)$ is equipped with,

$$norm \|f\|_k = \left[\sum_{s=0}^{k} \sum_{|\alpha|=s} \left\| \frac{\partial^{|\alpha|} f}{\partial x_1^{\alpha_1} \partial x_2^{\alpha_2} ... \partial x_{n_{sd}}^{\alpha_{n_{sd}}}} \right\| \right]^{\frac{1}{2}} \tag{31}$$

Therefore $L^2(\Omega)$ is, a *Sobolev* space, $H^0(\Omega)$. The *Sobolev* space for $k = 1$ is defined by,

$$H^1(\Omega) = \left\{ f \in L^2(\Omega) | \frac{\partial f}{\partial x_i} \in L^2(\Omega) \ i = 1, ..., n_{sd} \right\} \tag{32}$$

Note that the subspace $H_0^1(\Omega) = \{f \in H^1(\Omega) | f = f_D = 0 \,\text{on}\, \Gamma\}$ represents the elements which possess a *square integrable first derivative* over the domain Ω and vanish on its boundary Γ. Moreover, its inner product and norm coincide with those of $H^1(\Omega)$.

Remark 2: Note that the *Sobolev* spaces, namely $H^0(\Omega) = L^2(\Omega)$, $H^1(\Omega)$ and $H_0^1(\Omega)$, are *Hilbert* spaces with their corresponding *inner product* (a *Hilbert* space is a linear space with an *inner product* in which all *Cauchy sequences* are *convergent* sequences). $H_0^1(\Omega)$ is usually defined as the *closure* of $C_0^{\inf}(\Omega)$ (the *set* of all *continuous functions* with *continuous derivatives* whose support is a *bounded subset* of Ω).

Definition 3: (Extension to Vector-Valued Functions): In the finite element analysis of *flow problems*, attention will not be given only to *scalar functions* but also to vector-valued functions (such as fluid velocity $\mathbf{u}$). For a vector-valued function with n_{sd} components, that is $\mathbf{u} : \Omega \to R^{n_{sd}}$, consider again the domain $\Omega \subset R^{n_{sd}}$, $(n_{sd} \geq 1)$. Denote by $\mathbf{H}^k(\Omega) = [H^k(\Omega)]^{n_{sd}}$ the space of vector functions with n_{sd} components $\mathbf{u}(u, w, v)$ for which each component $u_i \in H^k(\Omega)$, $1 \leq i \leq n_{sd}$. The space $\mathbf{H}^k(\Omega)$ is equipped with an *inner product* inducing the following,

$$norm\|\mathbf{u}\|_k = \sqrt{\sum_{i=1}^{n_{sd}} \|u_i\|_k^2} \tag{33}$$

Definition 4: (Trial Solutions and Weighting Functions): To define the *weak* or variational form of a boundary value problem, we need to define two collections of functions, the *test* or *weighting* functions and the *trial* or *admissible* solutions. For instance in *standard Galerkin formulation*, the first collection of functions denoted by "V", is composed of *test functions* and consists of all functions which are square integrable, have square integrable first derivatives over the computational domain Ω, and *vanish* on the Dirichlet portion, Γ_D, of the boundary. The second collection of functions is called the *trial solutions*. This collection is similar to the test functions except that these *admissible* functions are required to satisfy the Dirichlet conditions on Γ_D. This second collection is denoted here by "S".

Remark 3: (Finite Dimensional Subsets): Note that the sets S and V clearly contain infinitely many functions. In the finite element method, S and V are approximated by convenient *finite dimensional subsets* of these collections which will be denoted by S^h and V^h. These finite element spaces are characterized by a partition of the domain (*triangulation* of the domain in FE element).

Definition 5: (Triangulation of the Domain in FE Element): The discretization of a domain Ω into element domains is triangulation. Let $\tau^h(\Omega)$ be a regular partition, also called *triangulation*, of Ω into n_{el} convex subdomains $\Omega^e \neq \Phi$, such that $\hat{\Omega} = \bigcup_{e=1}^{n_{el}} \hat{\Omega}^e$ and $\Omega^{e_1} \bigcap \Omega^{e_2} = \Phi$ for an element $e_1 \neq e_2$. Each subdomain Ω^e has a piecewise smooth boundary $\Gamma_e = \partial\Omega^e$, and h is a characteristic mesh size $diam(\Omega^e) \leq h$ (for all elements). The weighting (test) functions $w^h \in V^h$ vanish on Γ_D. The approximation (trial) u^h lies in S^h and satisfies, with the precision given by the characteristic mesh size h, the boundary condition u_D on Γ_D. In fact, along Γ_D we should have $u^h = U_D^h$. Moreover, the interpolation spaces are defined as,

$$V^h := \{w \in H^1(\Omega) | w|_{\Omega^e} \in P_m(\Omega^e) \forall e \,\text{and}\, w = 0 \,\text{on}\, \Gamma_D\} \tag{34}$$

$$S^h := \{w \in H^1(\Omega) | w|_{\Omega^e} \in P_m(\Omega^e) \forall e \text{ and } u = u_D \text{ on } \Gamma_D\} \tag{35}$$

where P_m is the *finite element interpolating space*. Note that V^h and S^h are finite dimensional subspaces of the spaces of test, V, and trial, S, functions.

3.2. **A Stabilized Galerkin/Least Square FEM for Unsteady Incompressible Flow.** Standard Galerkin finite element analysis of incompressible flows can introduce two main sources of potential numerical instabilities. The first one is due to the presence of nonlinear and non-symmetric advection terms in the governing equations (Equation 2), and can result in spurious oscillations in the velocity field. Such difficulty increases with the value of the flow's Reynolds number. High Reynolds number flows are convection dominated and the standard Galerkin formulation is unstable. Stabilization techniques must be used to provide *reliable* finite element solutions at high Reynolds numbers [10]. Addition instability can occur due to the incompressibility of the fluid (the incompressibility condition given by Equation 1) and appear when using inappropriate combinations of element interpolation functions to represent the velocity and pressure fields. As a consequence, instabilities in the pressure field may appear. A proper combination of interpolation spaces (for velocity and pressure) is needed. The Stabilized Galerkin/Least-Square (GLS) finite element formulation is used here in order to prevent such numerical instabilities (details on this technique can be found in the articles of Tezduyar et al [10, 20, 27, 28, 29]). In the present work, this stabilized finite element formulation was utilized using equal-order interpolation velocity-pressure elements as proposed by [29].

The formulation assumes that the spatial domain is fixed in time. This implies that the subscript t is dropped from the symbols Ω_t and Γ_t [27]. Contrary to the Galerkin or SUPG methods, where finite element spatial discretization being achieved first and the obtained discrete system discretized in time using *finite differences techniques* such the *θ-family* methods ($1 \leq \theta \leq 0$), the particularity of the ST-GLS, however, is the discretization of a so-called *space-time* domain using finite element discretization for time and space together (such a procedure was first used for the *discontinuous Galerkin* method [10]).

In the space-time finite element formulation, the time interval $(0, t_{max})$ is partitioned into subintervals $I_n = (t_n, t_{n+1})$, where t_n and t_{n+1} belong to an ordered series of time levels $0 = t_0 < t_1 < ... < t_N = t_{max}$. The space-time slab Q_n is defined as the space-time domain $\Omega \times I_n$. The lateral surface of Q_n is denoted by P_n; this is the surface described by the boundary Γ, as t traverses I_n. Similarly, P_n is decomposed into $(P_n)_D$ and $(P_n)_N$ with respect to the type of boundary condition being imposed (as shown in Equation 3, here we have only the Dirichlet part, including the interface, thus $(P_n)_D = P_n$). Finite element discretization of a space-time slab Q_n is achieved by dividing it into elements Q_n^e, $e = 1, 2, ..., (n_{el})_n$. $(n_{el})_n$ is the number of elements in the space-time slab Q_n.

The weak form of unsteady Navier-Stokes equations requires the introduction of classes of functions for the velocity field and the pressure field with respect to velocity $\mathbf{u}^h$. The space of trial solutions is denoted by $(S^h_{\mathbf{u}})_n$ and candidate approximating functions must satisfy a priori Dirichlet boundary conditions, on $(P_n)_D$ (recall here we have $(P_n)_D = P_n$). The trial solution space $(S^h_{\mathbf{u}})_n$ containing the approximating functions for the velocity is characterized as follows,

$$(\mathbf{S}^h_{\mathbf{u}})_n = \{\mathbf{u}^h | \mathbf{u}^h \in (\mathbf{H}_0^{1h}(Q_n) = [H_0^{1h}(Q_n)]^{n_{sd}}),\ \mathbf{u}^h = \mathbf{u}^h_D = 0 \text{ on } (P_n)_D\} \tag{36}$$

$\mathbf{H}_0^{1h}(Q_n)$ is the finite-dimensional function space over the space-time slab Q_n, with $\mathbf{H}_0^{1h}(Q_n) \subset \mathbf{H}_0^1(Q_n)$. This space is formed by using, over the parent (element) domains, *first-order* polynomials in space and time. The interpolation functions are continuous in space but

discontinuous in time. $\mathbf{H}_0^1(Q_n)$ denotes the Sobolev space over Q_n of square-integrable functions with square integrable first derivatives and zero value on the boundary $(P_n)_D$. The *weighting functions* of the velocity, $\mathbf{w}^h$, belong to $(\mathbf{V}_\mathbf{u}^h)_n$. Functions in this class have the same characteristics as those in class $(\mathbf{S}_\mathbf{u}^h)_n$, except that the weighting functions are required to vanish on $(P_n)_D$. The class $(\mathbf{V}_\mathbf{u}^h)_n$ is thus defined by,

$$(\mathbf{V}_\mathbf{u}^h)_n = \{\mathbf{w}^h | \mathbf{w}^h \in (\mathbf{H}_0^{1h}(Q_n) = [H_0^{1h}(Q_n)]^{n_{sd}}),\ \mathbf{w}^h = 0 \,\text{on}\, (P_n)_D\} \tag{37}$$

In the present study, since spatial derivatives of pressure do not appear in the weak form of the unsteady Navier-Stokes problem, the functions in $(S_p^h)_n$ are simply required to be *square-integrable* [10]. Moreover, since there are no explicit boundary conditions on pressure, the space $(S_p^h)_n = L^{2h}(Q_n)$ suffices as the *trial solution space* $(S_p^h)_n$ and as the weighting function space $(V_p^h)_n$. Note that in the present study, with *purely* Dirichlet velocity boundary conditions (Equation 3), the pressure is defined up to a constant. In such a case, its value must be prescribed at a given point of the time slab $Q_n = \Omega \times I_n$ (here the pressure, $p = 0$, is prescribed at the origin of coordinates). The pressure space is thus replaced by $(S_p^h)_n = (V_p^h)_n = L^{2h}(Q_n)/R$. Thus for pressure we introduce,

$$(S_p^h)_n = (V_p^h)_n = \{q^h | q^h \in (L^{2h}(Q_n))/R\} \tag{38}$$

Note that $L^{2h}(Q_n)$ is the finite-dimensional function space over the space-time slab Q_n, with $L^{2h}(Q_n) \subset L^2(Q_n)$. $L^2(Q_n)$ is the space of functions that are square integrable over the domain Q_n.

3.2.1. *ST-GLS Stabilization:* In order to illustrate the purpose of ST-GLS stabilization and to compare it with Galerkin method, lets consider the initial boundary problem given by Equations 1, 2, 3 and 4 along with the initial velocity field assumed as *divergence-free*, $\nabla \cdot \mathbf{u}_0 = 0$. The *weak formulation* is obtained, by projection of the Equations 1, 2, 3 and 4 onto a space of weighting functions $\mathbf{w} \in \mathbf{V}_\mathbf{u}$ for the momentum equation and $q \in V_p$ for the incompressibility condition (continuity). The result is the following Galerkin variational problem.
Given $\mathbf{F}$, $\mathbf{u}_D$, t and $\mathbf{u}_0$, find $\mathbf{u}(\mathbf{x}, t) \in \mathbf{S}_\mathbf{u}$, $\forall t \in (0, t_{max})$ and $p(\mathbf{x}, t) \in S_p$, $\forall t \in (0, t_{max})$, such that for all $\mathbf{w} \in \mathbf{V}_\mathbf{u}$, $q \in V_p$,

$$\int_\Omega \mathbf{w} \cdot \rho\left(\frac{\partial \mathbf{u}}{\partial t} + \mathbf{u} \cdot \nabla \mathbf{u}\right) d\Omega + \int_\Omega \epsilon(\mathbf{w}) : \boldsymbol{\sigma}(p, \mathbf{u}) d\Omega + \int_\Omega q \nabla \cdot \mathbf{u} d\Omega - \int_\Omega \mathbf{w} \cdot \mathbf{F} d\Omega = \int_{\Gamma_N} \mathbf{w} \cdot \mathbf{h}_N d\Gamma = 0 \tag{39}$$

with $\mathbf{u}_0 = \mathbf{0}$.
Its spatial Galerkin finite element discretization is given as,
Given $\mathbf{u}_D^h$, find $\mathbf{u}^h \in \mathbf{S}_\mathbf{u}^h$, $\forall t \in (0, t_{max})$ and $p(\mathbf{x}, t) \in S_p^h$, $\forall t \in (0, t_{max})$, such that for all $\mathbf{w}^h \in \mathbf{V}_\mathbf{u}^h$, $q^h \in V_p^h$, we have the *discrete system*,

$$\int_\Omega \mathbf{w}^h \cdot \rho\left(\frac{\partial \mathbf{u}^h}{\partial t} + \mathbf{u}^h \cdot \nabla \mathbf{u}^h\right) d\Omega + \int_\Omega \epsilon(\mathbf{w}^h) : \boldsymbol{\sigma}(p^h, \mathbf{u}^h) d\Omega + \int_\Omega q^h \nabla \cdot \mathbf{u}^h d\Omega - \int_\Omega \mathbf{w}^h \cdot \mathbf{F} d\Omega = \int_{\Gamma_N} \mathbf{w}^h \cdot \mathbf{h}_N d\Gamma = 0 \tag{40}$$

The discretization in time of this *discrete system* will be followed using finite difference techniques.

The GLS technique is defined by imposing that the stabilization term added is an *element-by-element* weighted least-squares formulation of the original Equation 2 to assure the numerical stability of the computations. This corresponds to the choice of an operator applied to the test function, $\mathcal{P}(w)$. With such a definition of operator $\mathcal{P}(w)$, the weak form must be solved. Therefore, the space-time formulation of Equations 1, 2, 3 and 4 can be written as follows,
Start with $(\mathbf{u}^h)_0^- = (\mathbf{u}_0)^h$, sequentially for $Q_1, Q_2, ..., Q_{N-1}$, given $(\mathbf{u}^h)_n^-$, find $\mathbf{u}^h \in (\mathbf{S}_{\mathbf{u}}^h)_n$ and $p^h \in (S_p^h)_n$, such that: $\forall \mathbf{w}^h \in (\mathbf{V}_{\mathbf{u}}^h)_n$ and $\forall q^h \in (V_p^h)_n$.

$$\begin{aligned}
&\int_{Q_n} \mathbf{w}^h \cdot \rho\Big(\frac{\partial \mathbf{u}^h}{\partial t} + \mathbf{u}^h \cdot \nabla \mathbf{u}^h\Big) dQ + \int_{Q_n} \boldsymbol{\epsilon}(\mathbf{w}^h) : \boldsymbol{\sigma}(p^h, \mathbf{u}^h) dQ \\
&\quad - \int_{(P_n)_N} \mathbf{w}^h \cdot \mathbf{h}_N dP + \int_{Q_n} q^h \nabla \cdot \mathbf{u}^h dQ - \int_{Q_n} \mathbf{w}^h \cdot \mathbf{F} dQ \\
&\quad + \int_{\Omega} (\mathbf{w}^h)_n^+ \cdot \Big((\mathbf{u}^h)_n^+ - (\mathbf{u}^h)_n^-\Big) d\Omega \qquad (41) \\
&+ \sum_{e=1}^{(n_{el})_n} \int_{Q_n^e} \boldsymbol{\tau}_{stab}^{GLS} \left[\rho\Big(\frac{\partial \mathbf{w}^h}{\partial t} + \mathbf{u}^h \cdot \nabla \mathbf{w}^h\Big) - \nabla \cdot \boldsymbol{\sigma}(q^h, \mathbf{w}^h) - \mathbf{F}\right] \\
&\quad \cdot \left[\rho\Big(\frac{\partial \mathbf{u}^h}{\partial t} + \mathbf{u}^h \cdot \nabla \mathbf{u}^h\Big) - \nabla \cdot \boldsymbol{\sigma}(p^h, \mathbf{u}^h) - \mathbf{F}\right] dQ = 0
\end{aligned}$$

Note that the term $\int_{(P_n)_N} \mathbf{w}^h \cdot \mathbf{h}_N dP$ vanishes since there no Neumann boundary condition ($\mathbf{h}_N = \mathbf{n} \cdot \boldsymbol{\sigma} = \mathbf{0}$). The coefficient $\boldsymbol{\tau}_{stab}^{GLS}$ determines the weight of added terms and is a matrix. In this time-space discretized form (discrete form), the following notation is being used [27, 28], $(\mathbf{u}^h)_n^{\pm} = \lim_{\delta \to 0} \mathbf{u}^h(t_n \mp \delta)$; $\int_{Q_n}(...)dQ = \int_{I_n}\int_{\Omega}(...)d\Omega dt$ and $\int_{P_n}(...)dP = \int_{I_n}\int_{\Gamma}(...)d\Gamma dt = 0$.

3.2.2. *Remarks on Stabilization:*

1. Comparing Equations 39 and 40 one can state that the least-squares *terms* added to the original Equation 2, to assure the numerical stability of the computations, are represented by the seventh integral in Equation 40. This is multiplied by the residual of Equation 2.
2. In the space-time formulation, Equation 40, the interpolation functions are discontinuous in time. The sixth integral enforces, weakly, the *continuity* of the velocity in time. The remaining series of integrals in Equation 40 are the terms added to the Galerkin variational formulation in the Q_n time slab.
3. This stabilization Galerkin/least-squares (GLS) procedure can be considered as a generalization of the stabilization based on the streamline-upwind/Petrov-Galerkin (SUPG) procedure employed for incompressible flows. It is with such stabilization procedures that it is possible to use elements that have *equal-order interpolation* functions for velocity and pressure that are otherwise unstable.
4. It is important to realize that the stabilizing terms added involve the momentum equation. Therefore, despite these additional terms, an exact solution is still admissible to the original Equation 2.
5. Based on a simple multidimensional generalization of the optimal τ_{stab}^{GLS}, given in [30]

for one dimensional space-time formulation, the coefficient τ_{stab}^{GLS} in the added stabilizing terms used in this formulation (first-order elements interpolations) is given as [27, 30]:

$$\boldsymbol{\tau}_{stab}^{GLS} = \left[\left(\frac{2}{\Delta t} \right)^2 + \left(\frac{2\|\mathbf{u}^h\|}{h} \right)^2 + \left(\frac{4v}{h^2} \right)^2 \right]^{-1/2} \tag{42}$$

v is the kinematic viscosity of the melt (solution), and Δt and h are the temporal and spatial finite element lengths (local mesh characteristics). $\|\mathbf{u}^h\| = \sqrt{(u^h)^2 + (v^h)^2}$ denotes the norm of the local velocity field vector (in the element). Note that other expressions may be found for $\boldsymbol{\tau}_{stab}^{GLS}$, for instance [20, 31].

6. The stability and accuracy analysis performed in [32], using Fourier analysis, indicates that for linear-in-time approximations (such as used here) the method is third-order accurate with respect to Δt and *unconditionally stable.*

7. The finite element interpolation functions are discontinuous in time. The fully discrete equations can be solved one space-time slab at a time (a fractional-step procedure). The memory needed for the global matrices involved in this method is quite extensive. Iteration methods can be employed to substantially reduce the cost involved in solving the linear equation systems arising from the space-time finite element discretization. Here, resolution was performed using iteration methods, for instance generalized minimal residual (GMRES) method [33].

3.3. **Stabilized Streamline Upwind Petrov-Galerkin (SUPG) Formulation for Heat Transport in the Liquid Phase.** Solutions to convection-dominated transport problems by the Galerkin method are often corrupted by *spurious node-to-node oscillations* [10, 34]. These can only be removed by extreme mesh and time-step refinement. This undermines the practical utilization of the method. Thus, for the heat transport equation, we also adopt the SUPG stabilization.

Consider the initial boundary value problem given by the unsteady convection-diffusion equation, Equation 5, and its associated boundary and initial conditions, Equations 6 and 7. Similar to the GLS technique, the principle of the SUPG stabilization technique is defined by taking a perturbation as the following.

$$\mathcal{P}(w) = \mathbf{u} \cdot \nabla w \tag{43}$$

This will introduced in the *weak form* of the problem, with w being the *weighting function.* The weak form of the initial value problem, Equations 5, 6 and 7, before introducing $\mathcal{P}(w)$, reads,

$$\int_\Omega w \left(\frac{\partial T}{\partial t} + \mathbf{u} \cdot \nabla T \right) d\Omega + \int_\Omega \nabla w \cdot (\alpha_L \nabla T) d\Omega - \int_{\Gamma_N} w h_T d\Gamma = 0 \tag{44}$$

When using $\mathcal{P}(w) = \mathbf{u} \cdot \nabla w$, the *perturbation* of the test function w, we obtained the *new weak* form given as,

$$\begin{aligned} &\int_\Omega w \left(\frac{\partial T}{\partial t} + \mathbf{u} \cdot \nabla T \right) d\Omega + \int_\Omega \nabla w \cdot (\alpha_L \nabla T) d\Omega \\ &+ \sum_{e=1}^{n_{el}} \int_{\Omega^e} \tau_{SUPG}^T (\mathcal{P}(w) \mathcal{R}(w)) d\Omega - \int_{\Gamma_N} w h_T d\Gamma = 0 \end{aligned} \tag{45}$$

$\mathcal{R}(w)$ is the residual of the equation of energy, Equation 5. $\mathcal{R}(w) = \partial T/\partial t + \mathbf{u} \cdot \nabla T - \nabla \cdot (\alpha_L \nabla T)$, since it is assumed no-source terms are considered in the obtaining of Equation

5. In fact, $\mathcal{P}(w)$ corresponds to the perturbation of the test function w firstly introduced in the Stream-Upwind method. The SU test function, $\tilde{w} = w + (\tilde{v}/\|\mathbf{u}\|^2)(\mathbf{u}\cdot\nabla w)$ [10], was consistently applied to all terms of the equation. Since the space of the test functions does not coincide with the space of the trial functions, this is a SUPG formulation.

Using suitably-defined finite-dimensional trial solution and weighting (test) function spaces given as,

$$S_T^h = \{T^h | T^h \in H^{1h}(\Omega),\, T^h = T_D \,\text{on}\, \Gamma_D\} \tag{46}$$

$$V_T^h = \{w^h | w^h \in H^{1h}(\Omega),\, w^h = 0 \,\text{on}\, \Gamma_D\} \tag{47}$$

The discrete problem can be obtained by finite element spatial discretization with restriction of the weak form, Equation 45. The *SUPG* method, with the perturbation $\mathcal{P}(w)$ defined in Equation 41 of the initial boundary problem, Equations 5, 6 and 7, can be written as follows.
Find $T^h \in S_T^h$ such that $\forall w^h \in V_T^h$,

$$\int_\Omega w\left(\frac{\partial T^h}{\partial t} + \mathbf{u}^h\cdot\nabla T^h\right)d\Omega + \int_\Omega \nabla w^h\cdot(\alpha_L\nabla T^h)d\Omega - \int_{\Gamma_N} w^h h_T d\Gamma$$
$$+\sum_{e=1}^{n_{el}}\int_{\Omega^e}\tau_{SUPG}^T(\mathbf{u}^h\cdot\nabla w^h)\left(\frac{\partial T^h}{\partial t} + \mathbf{u}^h\cdot\nabla T^h - \nabla\cdot(\alpha_L\nabla T^h)\right)d\Omega = 0 \tag{48}$$

Here n_{el} is the number of elements and Ω^e is the element domain corresponding to element e. τ_{SUPG}^T is the SUPG stabilization parameter, which is a scalar, (called the *intrinsic* time). In the numerical simulations, we use linear element interpolation for the temperature according to the method in [20]. The *stabilization parameter* τ_{SUPG}^T can be defined as,

$$\tau_{SUPG}^T = (\bar{v}/\|\mathbf{u}\|^2)) \tag{49}$$

$$\bar{v} = \beta h\|\mathbf{u}\|/2 \quad \text{(for elements interpolation used here for temperature)} \tag{50}$$

β is defined in terms of the Peclet cell number, $\beta = \coth(Pe - 1/Pe)$. For linear element interpolation of temperature,

$$\tau_{SUPG}^T = \frac{h}{2\|\mathbf{u}\|}\coth(Pe - 1/Pe) \tag{51}$$

Note that several expressions can be found for the stabilization parameter in the literature, for instance [2, 20, 33].

Finally, the finite element discretization of this weak form, Equation 48, yields a system of semi-discrete equations for $t \in (0, t_{max})$. In order to trace the transient response, this system of semi-discrete equations can be advanced in time by suitable finite difference schemes such as the θ family methods. A fully implicit method known as "Backward Differentiation Formulas" (BDF) is used [33].

3.4. **SUPG Formulation for Solute Transport Equation.** The same SUPG stabilization technique is used for the solute transport equation. Using suitably-defined finite-dimensional trial solution and test function spaces,

$$S_C^h = \{C^h | C^h \in H^{1h}(\Omega),\, C^h = C_D^h = C_{sat} \,\text{on}\, \Gamma_D,\, (\Gamma_D = \Gamma_{int}),\, \text{and}$$
$$\mathbf{n}\cdot D_L\nabla C^h = h_C = 0 \,\text{on}\, \Gamma_N\} \tag{52}$$

$$V_C^h = \{w^h | w^h \in H^{1h}(\Omega),\, w^h = 0 \,\text{on}\, \Gamma_D\} \tag{53}$$

The stabilized finite element formulation of the previous species equation, Equation 8, with boundary and initial conditions can be written as follows.
Find $C^h \in S_C^h$ such that $\forall w^h \in V_C^h$,

$$\int_\Omega w^h \left(\frac{\partial C^h}{\partial t} + \mathbf{u}^h \cdot \nabla C^h \right) d\Omega + \int_\Omega \nabla w^h \cdot (D_L \nabla C^h) d\Omega - \int_{\Gamma_N} w^h h_C d\Gamma$$
$$+ \sum_{e=1}^{n_{el}} \int_{\Omega^e} \tau_{SUPG}^C (\mathbf{u}^h \cdot \nabla w^h) \left(\frac{\partial C^h}{\partial t} + \mathbf{u}^h \cdot \nabla C^h - \nabla \cdot (D_L \nabla C^h) \right) d\Omega = 0 \tag{54}$$

where τ_{SUPG}^C is the SUPG stabilization parameter (for the solute transport equation).

3.5. **Numerical resolution.** After spatial discretization of the weak forms of the governing equations, a system of nonlinear ordinary differential equations is obtained for the solution of the velocity $\mathbf{u}$, the pressure p, the temperature T, and the solute concentration C. These are the discretized equations for the convective flow field, driven by both thermal/solutal buoyancy and magnetic body forces. Computations were carried out with the aid of the COMSOL Multiphysics package [33].

4. Simulation results and discussion

The simulations performed for the present crucible configuration, without magnetic field, exhibited an expected diffusion-dominated behavior in the dissolution process. Transport into the melt is relatively slow and continues to slow down as the concentration gradient flattens. The silicon source placed at the top of the melt dissolves under the applied temperature profile into the germanium melt in the opposite direction to the gravity-induced buoyancy force. Due to the large density difference between the silicon solute and the germanium-rich melt, the areas of melt high in silicon solute concentration are buoyant. Therefore, the diffusion of silicon acts to stabilize the melt against natural convection. This makes the silicon transport in these systems diffusion dominated, and naturally leads to slower growth rates.

The stable flow structure, caused by silicon buoyancy in the melt, results in a very flat dissolution interface. However, in the presence of an applied static magnetic field, the shape of the dissolution interface is significantly different as seen in Figure 3. While the interface is flat everywhere under no magnetic field, with application of the magnetic field, areas near the crucible wall experience a higher dissolution rate and more material is removed into the melt.

The interface remains flat at the center of the material. However, near the wall the interface slightly curves into the material. There is more dissolution in this region than the center. This indicates a significant alteration to the melt flow structure. The upward strong hot convective flows, due to the action of combined thermosolutal buoyancy and magnetic body forces observed in the crucible near the heated lateral surface, hit the interface at the edges and contribute to the solute transport near this region. Some of these hot upward flows turn away to the center of the crucible and hence bring the diffused solute away from the edge to the center of the bulk melt. In the region close to the center of the interface, the convective flow is very weak. This is due to the domination of the diffusion in this region. The flow structure under various magnetic fields are illustrated in Figures 4, 5 and 6.

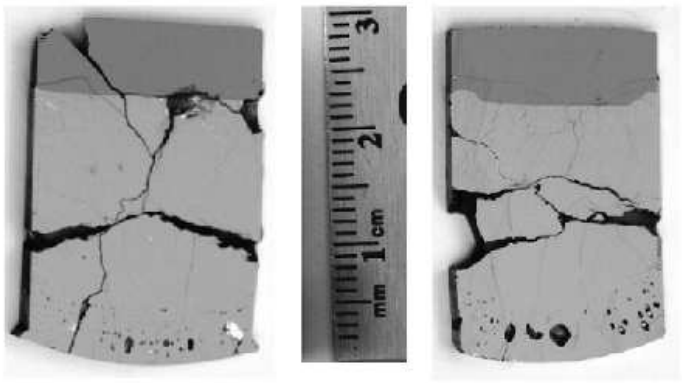

FIGURE 3. Experiment conducted with no field on the left and experiment conducted with field is on the right. The regions of high dissolution are easily visible under magnetic field.

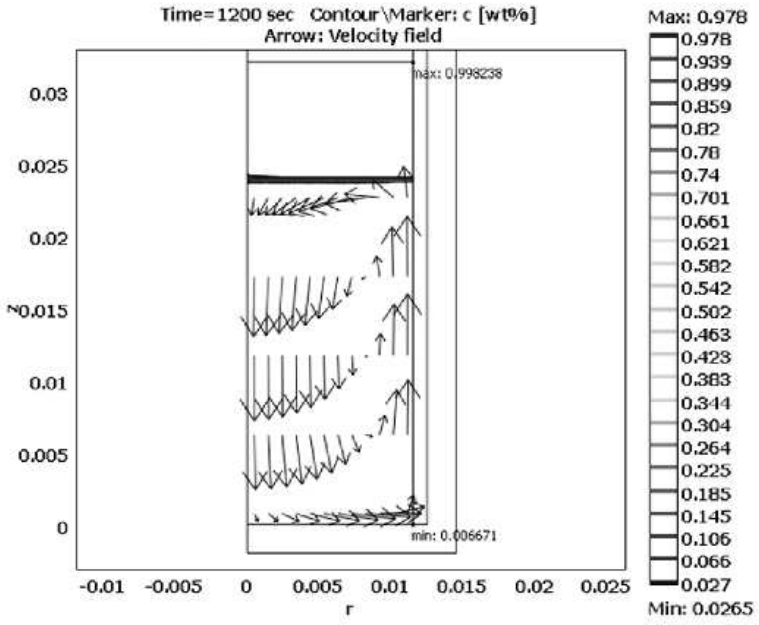

FIGURE 4. Simulation after 30min with no applied field. Arrows indicate flow structure, and isolines illustrate concentration profile. The profile around the dissolution interface is flat.

The magnetic field appears to be acting to mix silicon away from the crucible wall and into the center. This action creates a higher concentration gradient at the crucible edge with increasing dissolution. Due to a slight increase in dissolved silicon, it appears that the applied field does not have a significant effect on the axial flow structure, this is well observed in the distribution of the axial velocity components, while the radial flow component appear to be increased (not presented here). These observations were supported by experiments [8]. Note that here we have performed the simulation using an axisymmetric model, for which tangential flow is ignored. The axisymmetric model does predict the flows structure well, but fails in predicting the interface evolution. Hence, the tangential

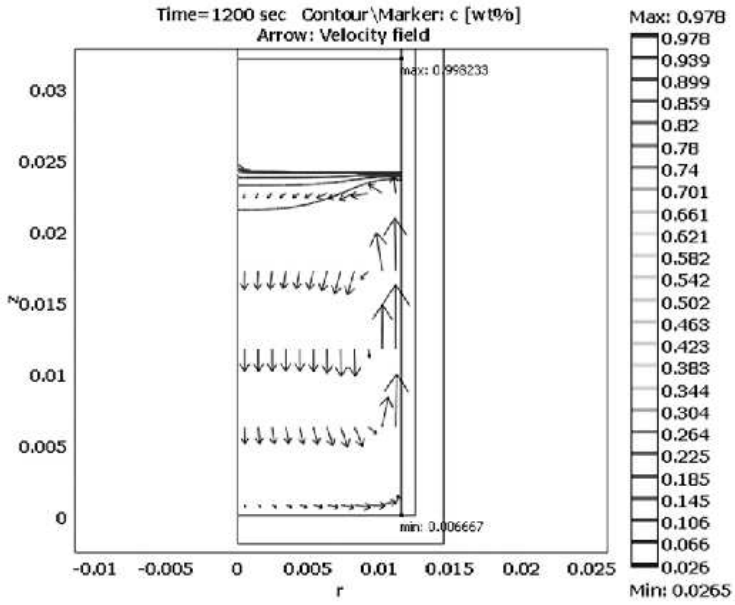

FIGURE 5. Simulation after 30min with 0.3T applied field. Arrows indicate flow structure, and isolines illustrate concentration profile. The profile around the dissolution shows that silicon is being mixed away from the crucible edge towards the center.

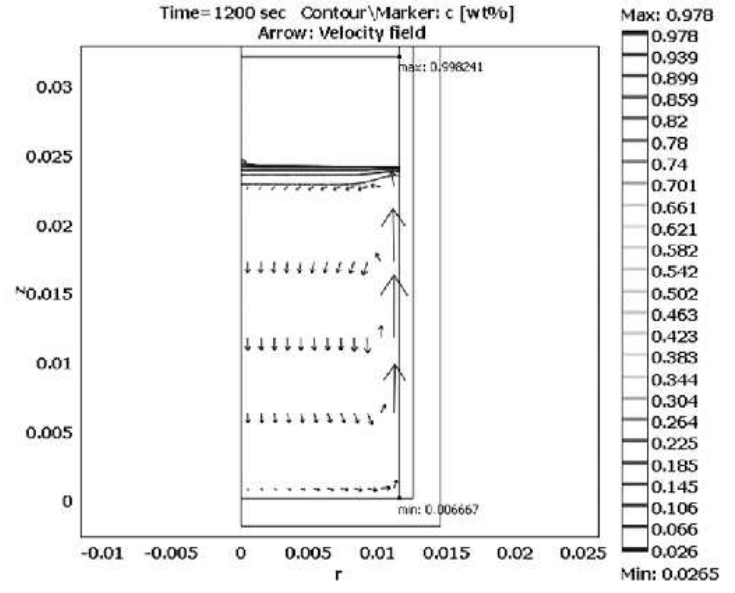

FIGURE 6. Simulation after 30min with 0.8T applied field. Arrows indicate flow structure, and isolines illustrate concentration profile. The profile around the dissolution shows that silicon is being mixed away from the crucible edge towards the center, but is less pronounced than the simulation with 0.3T applied field.

flows have a significant impact on the evolution of the dissolution interface. This impact

of the tangential flows was well emphasized experimentally by Armour and Dost in [8].

It is well known that a static magnetic field is frequently utilized to suppress thermosolutal convection in crystal growth. In the present crucible configuration, it appears that the flow is not suppressed. Instead, the applied magnetic field enhances the already weak stable flow structure. Indeed, the applied field strengthens the upward flow near the lateral heated crucible wall and damps the downward flow in the crucible core. An external magnetic field, aligned perfectly with the axis of the growth cell (z-direction), gives rise to a magnetic body force in the horizontal plane that balances the vertical gravitational body force, and consequently may weaken the convective flow.

The present numerical simulations confirm the suggestions pointed out in [8]. The observed dissolution structure may be advantageous to the LPD crystal growth of SiGe, where the curvature of the growth interface evolves with growth. It may be possible to use this effect to better control interface shape.

5. Conclusions

The numerical simulations conducted here using an axisymmetric model lead to the following conclusions. Transport in a silicon-germanium system, where silicon is being dissolved from the top of the melt, exhibits a diffusion-dominated behavior. As has been previously explained numerically [21] and experimentally [8], this is due to the silicon species buoyancy in the germanium melt. As predicted, in an isothermal system the transport does appear to proceed in a diffusion-dominated manner.

In the dissolution process considered here, the application of a static magnetic field to the melt does not weaken the strength of the flow structure (near the lateral heated crucible wall). As the system is already relatively free of thermosolutal convection, the applied magnetic field leads to strengthening the radial and tangential (neglected here) flow components. This appears to cause significant mixing of silicon away from the crucible wall into the core of the melt. This phenomenon may be utilized in controlling growth interface geometry. Specifically, it may be utilized to maintain a constant growth interface curvature during the LPD growth cycle.

Axial mixing does not appear to significantly increase and the concentration profile seems to evolve as diffusion-dominated system. The chosen value of silicon diffusivity $D^{Si} = 2.5 \times 10^{-8}\, m^2/s$ agrees well with experiments. The numerical results of the present setup show that the silicon dissolution was slightly enhanced under an applied vertical magnetic field. This enhancement peaked for the field levels between 0.3 and 0.5 Tesla. The magnetic field level of 0.8 Tesla is a good choice for obtaining a uniform concentration distribution. This observation can be attributed to the altered flow structure in the melt due to the magnetic field. Finally by comparing numerical results with experiments, one may state that the axisymmetric model may predict the flow structure. However, the computed dissolution interface did not agree with experiments. This could be due to the tangential flows having a significant impact on the evolution of the dissolution interface. Thus, three-dimensional simulations are required for the present growth system.

Acknowledgement: We gratefully acknowledge the financial support provided by the Canadian Space Agency (CSA), Canada Research Chairs (CRC) Program, and the Natural Sciences and Engineering Research Council (NSERC) of Canada.

References

[1] Dost, S. and Lent, B., (2007), Single Crystal Growth of Semiconductors from Metallic Solutions, Elsevier, Amsterdam, the Netherlands.

[2] Hauke, G., (2002), A simple subgrid scale stabilized method for the advection-diffusion-reaction equation, Comput. Methods Appl. Mech. Engrg. 191, 2925-2947.

[3] Muller, G. and Ostrogorsky, A.G., (1994), Convection in melt growth. In Handbook of Crystal Growth. (ed. D.T.J. Hurle), North-Holland, Amsterdam, vol. 2, p. 711-814.

[4] Deal, A., (2004), Enhanced morphological stability in Sb-doped Ge single crystals, PhD thesis, Florida University, USA.

[5] Hurle, D. T. J., (1973), Melt Growth chapter in Crystal Growth, edited by P. Hartman, North-Holland, Amsterdam.

[6] F. Mechighel (2010): Modélisation de la convection au cours de changement de phase liquide-solide: effet d'un champ magnétique, PhD thesis University of Limoges, France.

[7] Ozoe, H., Szmyd, J. S. and Tagawa,T., (2007), Magnetic Fields in Semiconductor Crystal Growth, S. Molokov et al. (eds.), Magnetohydrodynamics - Historical Evolution and Trends, 375-390, Springer.

[8] Armour, N. and Dost, S., (2009), Effect of an applied static magnetic field on silicon dissolution into a germanium melt, Journal of Crystal Growth, 311, 780-782.

[9] Sistek, J., (2008), The finite element method in fluids: stabilization and domain decomposition Ph.D. thesis, Czech Technical University in Prague.

[10] Donea, J. and Huerta, A., (2003), Finite Element Methods for Flow Problems, John Wiley and Sons, Ltd.

[11] Polner, M., (2005), Galerkin Least-Squares Stabilization Operators for the Navier-Stokes Equations A Unified Approach, PhD thesis, University of Twente, The Netherlands.

[12] Franca, L. P., Frey, S. L. and Hughes, T. J. R., (1990), Stabilization Finite Element Methods: I. Applications to the advective-diffusive model, INRA research report (N. 1300), France.

[13] Brooks, A. N. and Hughes, T. J. R., (1982), Streamline Upwind/Petrov-Galerkin formulations for convective dominated flows with particular emphasis on the incompressible Navier-Stokes equations, Comput. Methods Appl. Mech. Engrg. 32, 199-259.

[14] Tezduyar, T. E. and Ganjoo, D. K., (1986), Petrov-Galerkin formulations with weighting functions dependent upon spatial and temporal discretization: Applications to transient convection-diffusuion problmes. Computer Methods in Applied Mechanics and Engineering, 59, 49-71.

[15] Hughes, T. J. R., Franca, L. P. and Hulbert, G. M., (1989), A new finite element formulation for computational fluid dynamics: VIII. The Galerkin-least-squares method for advective-diffusive equations, Comput. Methods Appl. Mech. Engrg. 73, 173-189.

[16] Feby, A., Behr, M. and Heinkenschloss, M., (2004), The effect of stabilization in finite element methods for the optimal boundary control of the Oseen equations, Finite Elements in Analysis and Design 41, 229-251.

[17] Hughes, T. J. R., (1995), Multiscale phenomena: Green's function, the Dirichlet-to-Neumann formulation, subgrid scale models, bubbles and the origins of stabilized formulations, Comput. Methods Appl. Mech. Engrg. 127, 387-401.

[18] Franca, L. P. and Farhat, C., (1994), Bubble functions prompt unusual stabilized finite element methods, Comput. Methods Appl. Mech. Engrg. 123, 299-308.

[19] Donea, J., (1984), A Taylor-Galerkin method for convection transport problems, Int. J. Numer. Methods Engrg. 20, 101-l19.

[20] Codina, R., (1998), Comparison of some finite element methods for solving the diffusion-convection-reaction equation, Comput. Methods Appl. Mech. Engrg. 156, 185-210.

[21] Yildiz, M., Dost, S. and Lent, B., (2005), Growth of bulk SiGe single crystals by liquid phase diffusion, Journal of Crystal Growth 280, 151-160.

[22] Yildiz, M., (2005), A Combined Experimental and Modeling Study for the Growth of SixGe1-x Single Crystals by Liquid Phase Diffusion (LPD), PhD thesis, University of Victoria, Canada.

[23] Yildiz, M. and Dost, S., (2005), A continuum model for the Liquid Phase Diffusion growth of bulk SiGe single crystals, International Journal of Engineering Science 43, 1059-1080.

[24] Yildiz, E., Dost, S. and Yildiz, M., (2006), A numerical simulation study for the effect of magnetic fields in liquid phase diffusion growth of SiGe single crystals, Journal of Crystal Growth, 291, 497-511.

[25] Yildiz, E. and Dost, S., (2007), A numerical simulation study for the combined effect of static and rotating magnetic fields in liquid phase diffusion growth of SiGe, Journal of Crystal Growth, 303, 279-283.

[26] Thess, A., Votyakov, E., Knaepen, B. and Zikanov, O., (2007), Theory of the Lorentz force flowmeter, New Journal of Physics, 9, 299-325.
[27] Tezduyar, T. E., (1992), Stabilized Finite Element Formulations for Incompressible Flow Computations, Advances in Applied Mechanics, vol. 28, 1-44.
[28] Tezduyar, T. E., Mittal, S. and Shih, R., (1991), Time-accurate incompressible flow computations with Quadrilateral velocity-pressure elements, computer methods in applied mechanics and engineering, 87, 363-384.
[29] Tezduyar, T. E., Mittal, S., Ray, S. E. and Shih, R., (1992), Incompressible flow computations with stabilized bilinear and linear equal-order-interpolation velocity-pressure elements, Computer Methods in Applied Mechanics and Engineering, 95, 221-242.
[30] Shakib, F., (1988), Finite element analysis of the compressible Euler and Navier-Stokes equations, Ph.D. Thesis, Department of Mechanical Engineering, Stanford University, Stanford, California.
[31] COMSOL Multiphysics Modeling Guide, COMSOL AB. (2007), SE-111 40 Stockholm.
[32] Shakib, F. and Hughes, T. J. R., (1991), A new finite element formulation for computational fluid dynamics. IX. Fourier analysis of space-time Galerkin/least-squares algorithms, Comput. Methods Appl. Mech. Eng. 87(1), 35-58.
[33] Saad, Y. and Schultz, M. H., (1983), GMRES: A generalized minimal residual algorithm for solving nonsymmetric linear systems. Yale University Research Report YALEU/DCS/ RR-254.
[34] Akin, E. J. and Tezduyar, T. E., (2004), Calculation of the advective limit of the SUPG stabilization parameter for linear and higher-order elements, Comput. Methods Appl. Mech. Engrg., 193, 1909-1922.
[35] Tezduyar, T. E. and Osawa, Y., (2000), Finite element stabilization parameters computed from element matrices and vectors, Comput. Methods Appl. Mech. Engrg., 190, 411-430.

Farid Michighel got his PhD from University of Limoges, France and University of Constantine, Algeria, 2010. His main research is in the area of computational modeling of crystal growth, with particular application to innovative techniques, such as Liquid Phase Diffusion, Bridgman, etc. Moreover, he is interested in domains such: solidification phenomena, with particular application to solidification processes relevant to the metallurgy industry, Magnetohydrodynamics (MHD), welding, and Sintering. Recently, he is interested in numerical modeling using Lattice Boltzmann method (LBM).

Neil Armour got his MSc from University of Victoria, 2005. He is currently a PhD candidate at University of Victoria. Mr. Armour's research is focused on bulk crystal growth of SiGe and its transport properties.

Sadik Dost is a Professor and Canada Research Chair in Semiconductor Crystal Growth, and Director of the Crystal Growth Laboratory at the University of Victoria. He has served as Founding Director of the university research center, Centre for Advanced Materials and Related Technology (CAMTEC) from 1992 to 1997, and also as Chair of the Department of Mechanical Engineering from 1997 to 2003. Dr. Dost has held a variety of potions in learned and professional bodies.

Mahfoud Kadja is a Professor of Mech. Eng. at the University of Constantine (Algeria) since 1998. His research interests include CFD, heat transfer and environmental flows. He has published papers in this field and has participated in many national and international conferences.